Tellus (1993), 45B, 228–241
Printed in Belgium – all rights reserved

TELLUS
ISSN 0280–6509

The atmospheric CH_4 increase since the Last Glacial Maximum

(1). Source estimates

By JÉRÔME A. CHAPPELLAZ*[1] and INEZ Y. FUNG, *NASA/Goddard Institute for Space Studies, 2880 Broadway, New York NY 10025, USA*, and ANNE M. THOMPSON, *NASA/Goddard Space Flight Center, Code 916, Greenbelt MD 20771, USA*

(Manuscript received 27 March 1992; in final form 9 November 1992)

ABSTRACT

An estimate of the distribution of wetland area and associated CH_4 emission is presented for the Last Glacial Maximum (LGM, 18 kyr BP, kiloyear Before Present) and the Pre-Industrial Holocene (PIH, 9000–200 years BP). The wetland source, combined with estimates of the other biogenic sources and sink, yields total source strengths of 120 and 180 Tg CH_4/yr for LGM and PIH respectively. These source strengths are shown to be consistent with source estimates inferred from a photochemical model, and point to changes in wetland CH_4 source as a major factor driving the atmospheric CH_4 increase from LGM to PIH.

1. Introduction

Methane is an important trace gas involved in the radiative budget and atmospheric chemistry. Methane measurements performed on air bubbles trapped in Greenland and Antarctic ice cores reveal a doubling of its atmospheric concentration from 350 ppbv (part per billion by volume) during the Last Glacial Maximum (LGM) to 650 ppbv during the Preindustrial Holocene (PIH) (Stauffer et al., 1988; Chappellaz et al., 1990), followed by an unprecedented increase during the last 2 centuries (Craig and Chou, 1982; Khalil and Rasmussen, 1982; Rasmussen and Khalil, 1984; Stauffer et al., 1985; Pearman et al., 1986; Raynaud et al., 1988). At present, the atmospheric CH_4 level is $\sim$1700 ppbv and is increasing at a rate of 0.8–1.0%/yr (Rasmussen and Khalil, 1986; Steele et al., 1987; Blake and Rowland, 1988). The future rate of increase and therefore the role of CH_4 in future climate remain uncertain as its budget is not well known. In particular, the natural source strengths and their link with climate change must be determined in order to estimate a potential feedback in the context of future warming.

There have been several recent attempts to analyze CH_4 budgets for the LGM and/or PIH (McElroy, 1989; Valentin, 1990; Crutzen and Zimmermann, 1991; Pinto and Khalil, 1991). These studies use photochemical models to estimate OH (hydroxyl radical) oxidation of CH_4 (i.e., the CH_4 lifetime) and infer source strengths required to produce the measured CH_4 concentrations deduced from ice cores. Because the models make varying assumptions about CO, NO_x, O_3, and temperature, thereby obtaining different OH distributions, the inferred CH_4 sources range from 90–180 Tg CH_4/yr for the LGM and 170–250 Tg CH_4/yr for the PIH. In contrast, we approach the historical CH_4 budget by making a direct and quantified estimate of methane sources and determining their consistency with atmospheric concentrations in a photochemical model. This paper addresses the source estimate with a focus on wetland changes from LGM to the present and gives photochemical model results demonstrating the self-consistency of this budget with the ice-core record. A companion paper (Thompson et al.,

* Permanent address: CNRS Laboratoire de Glaciologie, BP 96, 38402 St Martin d'Hères Cedex, FRANCE.
[1] Corresponding author.

1993) describes the photochemical calculations in more detail and focuses on the consequences of CH_4 emission changes for LGM and PIH atmospheric chemical composition.

2. Methane sources and soil sink

The basis for our present-day CH_4 budget is a recent three-dimensional model synthesis (Fung et al., 1991) which is constrained by all the available CH_4 observations, i.e., the geographical and seasonal distribution of atmospheric CH_4, its isotopic composition, the strength and geographical distribution of some sources, and the modelled three-dimensional global distribution of OH (Spivakovsky et al., 1990a, b). We consider their preferred budget scenario which satisfies most of the constraints; it includes a global annual source of 500 Tg, with 115 Tg from wetlands, 55 Tg from biomass burning, 80 Tg from animals, and 20 Tg from termites. The remainder of the sources are from rice cultivation, landfills, and from coal and gas exploration and transmission. Of the 460 Tg/yr sink, 450 Tg/yr is caused by chemical destruction in the atmosphere and 10 Tg/yr is attributed to consumption of methane in dry soils. In the following, we start with the methane sources and sinks for today, and estimate how each has been altered for the PIH and LGM.

There are few direct and global observations of the components of the natural CH_4 budget on the time scale considered here. For the PIH, we surveyed historical information about human impacts on the biosphere and deduced changes in source activities and methane flux.

For LGM, direct information on the extent and distribution of wetlands, the largest single CH_4 source, is sparse and generally not quantified (e.g., Petit-Maire et al., 1991). While the existence of wetlands is predicated on positive water balance and high moisture retention by the soils, there is no scheme that predicts wetland distribution based on climate. Here we use today's distributions to establish wetland occurrence as a function of two correlates: the dominant vegetation type, as a broad indicator of hydrologic, climate and edaphic conditions; and the slope of the terrain, a major control of drainage and runoff. The vegetation distribution for the LGM is then used together with the topography to predict the wetland distribution of the LGM. Similarly, our strategy for estimating the other LGM sources also uses vegetation and its changes as a proxy. The vegetation and slope data are described below.

Vegetation. Because vegetation is an identifying characteristic of wetlands, we categorize wetland distribution into several groups based on their vegetation association, and investigate how wetland areas in each group have changed. There are several digital databases of today's vegetation distribution to facilitate our analysis (Matthews, 1983; Henderson-Sellers and Wilson, 1983). However, there is only one published global vegetation map for the LGM (Adams et al., 1990). We note that vegetation distributions for today and LGM have also been modelled using bioclimatic schemes (Prentice, 1990; Prentice and Fung, 1990). However, uncertainties in the modelled climate for the LGM (Rind and Peteet, 1985) would cloud the interpretation of vegetational and other changes. We thus use the Adams vegetation maps for today and the LGM as the basis for our analysis.

The vegetation classification of Adams et al. (1990) consists of 24 vegetation types, grouped into 12 types in their published maps. The LGM vegetation distribution was reconstructed based on palynological, pedological and sedimentological paleodata. We digitized the maps for both today and the LGM at $1^\circ \times 1^\circ$ resolution for our analysis. As the projection of the original maps was unknown, the vegetation data base of Matthews (1983) was used as a guide for the digitization. This procedure results in areal estimates of each vegetation type that are slightly different from those published. However, as visual comparison of the digitized and published maps was favorable, and the projection of the digitized maps was known, the updated areal estimates were deemed more accurate (J. Adams, personal communication).

Terrain slope. Wetland ecosystems are often found in flat or relatively flat ground, where runoff is impeded or at slow enough a rate so that anoxic conditions in the soil can exist. Therefore, the slope of the terrain provides a quantitative constraint for selecting regions of potential wetland occurrence. The ETOP05 data set (NGDC, 1988) combines bathymetry data from the US Naval Oceanographic Office with land elevations obtained from

remote sensing and national surveys. Although the grid spacing of the data base is $5' \times 5'$, the information is at $5' \times 5'$ only for the oceans, the contiguous United States, Japan, Western Europe, New Zealand and Australia; and is at $10' \times 10'$ elsewhere (NGDC, 1988). From this high-resolution data set, we computed the mean slope within each $1° \times 1°$ grid.

Terrain slopes for the LGM were calculated using the ETOP05 data set with a sea-level drop of 130 m (Fairbanks, 1989) and with the continental ice sheets added (CLIMAP Project Members, 1981).

2.1. *Wetlands*

Anaerobic decomposition of organic matter in wetlands is the most important natural source of methane, comprising 15–25% of the global methane source today. Estimation of the global annual methane emission from this source requires information about (1) the areal extent of wetlands; (2) the period of inundation or methane production during the year; and (3) the rate of methane emission to the atmosphere during the production period.

2.1.1. Distribution of wetlands for today. For today, the global distribution of wetlands was compiled from existing maps and data bases using information about vegetation, soil and inundation characteristics (Matthews and Fung, 1987; Aselmann and Crutzen, 1989). The global wetland area estimated by these authors is 5300×10^9 m^2 and 5700×10^9 m^2, respectively. Differences between the two studies lie essentially in the Amazon basin, Australia, Alaska and Canada (see Aselmann and Crutzen, 1989, for a discussion). However the latitudinal distributions match fairly well: the wetlands are mainly distributed into two latitudinal bands, between 70° and 50°N and between 20°N and 30°S. In our analysis, we use the global data base at 1° resolution of Matthews and Fung (1987).

Wetland/vegetation relationship. Today's distribution of wetland area among the vegetation types of Adams et al. (1990) is given in Fig. 1a and Table 1. Because of their large expanse, 24% of the total wetlands are associated with boreal conifer forests. Temperate and tropical forests and woodlands also include a large fraction of the global wetland area (50% all together) whereas, as expected, a small part is associated with arid

Table 1. *Present-day relationship between wetlands and vegetation groups and between wetlands and slope of terrain*

Vegetation type (Adams et al., 1990)	% of global wetland area today (PIH)	Distribution (%) of wetlands in each slope class (%) 0–0.2	0.2–0.4	0.4–0.6	0.6–0.8	0.8–1.0	1.0–more
tropical moist forest	11.2 (11.8)	63.5	10.2	5.1	2.6	3.0	15.5
tropical scrub/woodland	16.5 (15.8)	52.1	22.5	8.8	6.2	2.9	7.6
grassland	10.1 (8.5)	66.3	21.9	5.4	2.0	1.4	2.9
semi-desert/steppe	2.6 (2.2)	63.9	10.9	6.1	2.8	0.7	15.6
temperate broad-leaved forest	8.1 (16.0)	66.4	24.2	4.7	0.3	2.6	1.7
boreal/conifer forest	24.2 (22.9)	47.6	21.6	13.6	5.6	3.5	8.2
open conifer woodland	14.0 (11.7)	53.2	18.9	12.8	4.3	3.2	7.6
tundra	11.4 (9.5)	41.7	19.2	9.3	6.0	5.1	18.7
polar desert	0.0 (0.0)	0.0	0.0	0.0	0.0	0.0	0.0
ice	0.0 (0.0)	0.0	0.0	0.0	0.0	0.0	0.0
desert	1.9 (1.6)	59.3	12.9	2.8	1.3	1.6	22.0
southern steppe/tundra	0.0 (0.0)	0.0	0.0	0.0	0.0	0.0	0.0
global	100.0 (100.0)	54.4	19.6	9.3	4.3	3.1	9.4

The calculations are based on wetland (Matthews and Fung, 1987), vegetation (Adams et al., 1990) and topography (NGDC, 1988) global datasets. Wetland area associated with polar desert (23×10^9 m^2) is rounded to zero.

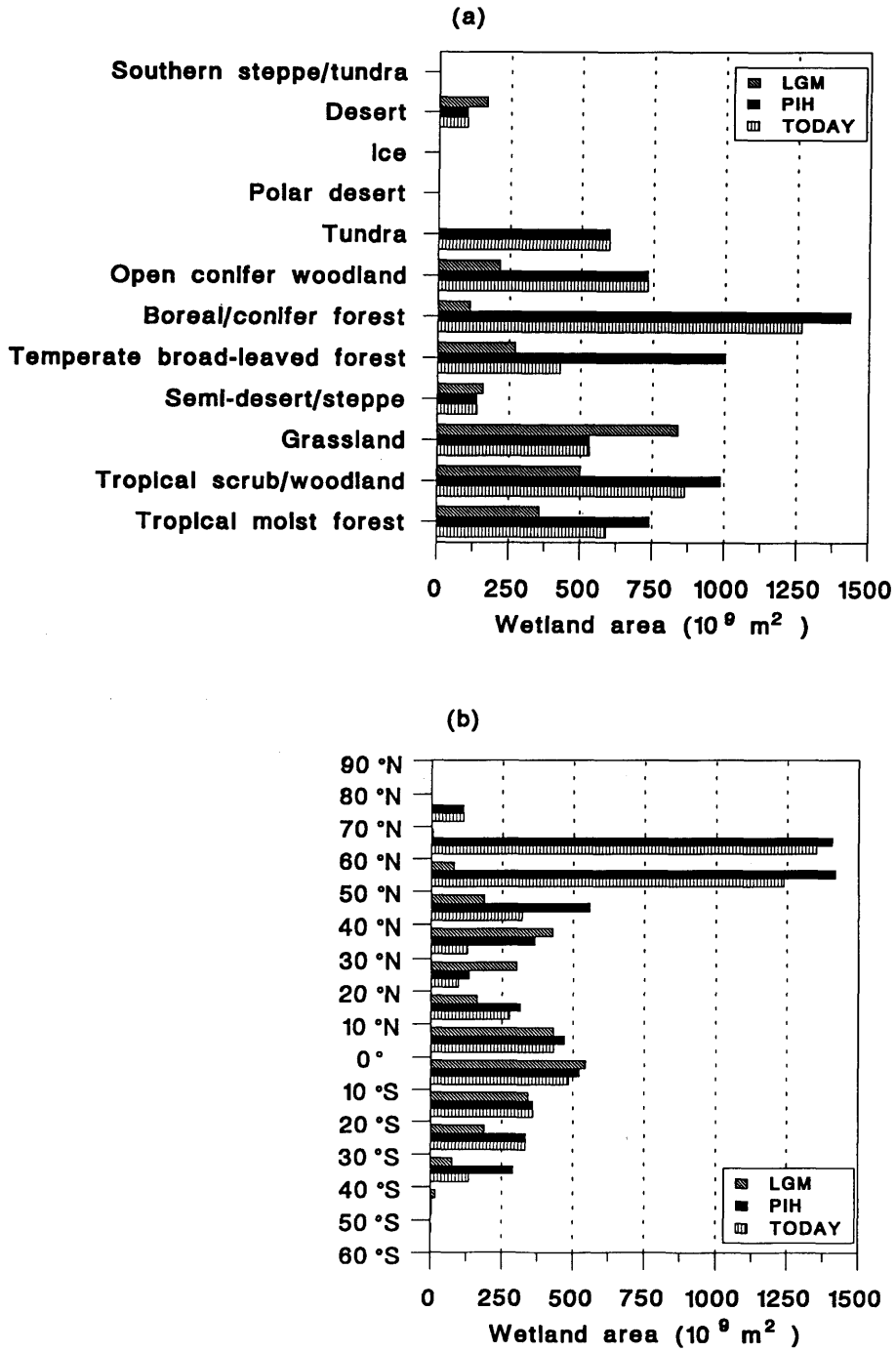

Fig. 1. (a) Global wetland area associated with broad vegetation groups for present-day, PIH and LGM. The vegetation groups are those defined in Adams et al. (1990). (b) Latitudinal distribution of wetland areas for present-day, PIH and LGM.

vegetation (less than 5% in semi-desert and desert). As has been discussed in Matthews and Fung (1987), about two-thirds of the global wetland area are scattered over the surface of the world, and occupy < 10% of many a 1° grid. Thus, they cover at most on the order of 10% of the total area of a given vegetation type: the wetland coverage is 8.9% for open conifer woodlands and tundra, 8.1% for boreal/conifer forests, and 4.8% for tropical moist forests. The inundated fractions are much lower in the arid/semi-arid vegetation: 3.7% for tropical scrub and woodlands, 3.0% for grasslands, 1.1% for semi-deserts and 0.5% for deserts.

Wetland/slope relationship. Fig. 2 illustrates the frequency distributions of wetland area and land surface area as a function of the slope of the terrain. About 54% of the present-day global wetland area is associated with a slope smaller than 0.2% (at 1° resolution); the percentage increases to 74% for slopes <0.4%. By contrast, 23 and 45% of the land surface are associated with slopes of <0.2% and 0.4%, respectively. As is expected, wetlands are mainly associated with small slopes.

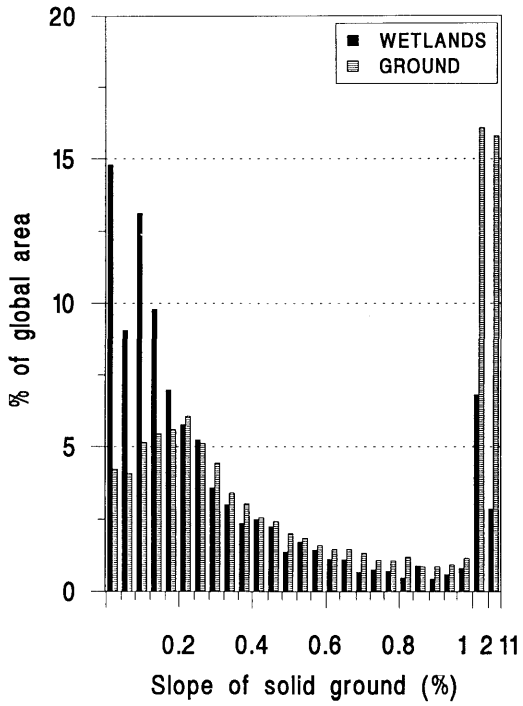

Fig. 2. Distribution of present-day wetland and land surface area as a function of mean terrain slope resolved at 1° resolution.

The frequency distribution of wetland areas for different vegetation groups and slope classes is shown in Table 1. For most vegetation groups, over half of the wetlands occurs in areas with slopes <0.2%. Although 26% of the global wetland area is found at slopes >0.4%, these wetlands are not scattered through the other vegetation groups; they are essentially found in conifer forests/woodlands and tundra. For example, about 1/5 of the wetlands associated with tundra are found at slopes steeper than 1.0%. For these wetlands on steep terrain, factors such as texture and water holding capacity of the soil may be important for explaining their occurrence. Also our slope calculation at 1° resolution cannot represent scattered depressions in the ground which can favor wetland occurrence in undulating landscapes (such as in Scandinavia and Alaska).

2.1.2. Distribution of wetlands for PIH. The population growth and demands in the last 200 years have resulted in a depletion of wetlands today. Wetlands were drained and converted for agricultural, residential and other uses. Also peat is exploited for fuel. To estimate the wetland area in the PIH, we carried out a survey of the history of wetland exploitation. The regions surveyed include: the contiguous United States, the Southern Taiga of Russia, Finland, United Kingdom, Australasia and South-Southeast Asia. These are described below.

The contiguous United States. Several estimates exist on the natural wetland extent in the presettlement time and a medium range is $600–750 \times 10^9$ m^2 (Roe and Ayres, 1954; Shaw and Fredine, 1956; Office of Technology Assessment, 1984; Mitsch and Gosselink, 1986). Today the figure is about 200×10^9 m^2 (Matthews and Fung, 1987; Aselmann and Crutzen, 1989). The Alaskan and Canadian wetlands have not been significantly altered by human activities so far (Armentano and Menges, 1986).

The Southern Taiga of Russia. Botch and Masing (1983) estimate that about 70% of the preexisting mires in this region have been reclaimed. From the data set of Matthews and Fung (1987), about 235×10^9 m^2 of bogs and

swamps are there today, suggesting a potential PIH area of 780×10^9 m^2 and a cultivation area of 545×10^9 m^2. However from land use data (Matthews, 1983), we find that only 155×10^9 m^2 are currently cultivated in the Southern Taiga. We use this more conservative figure as the converted wetland area in the region since PIH.

Finland. Ruuhijärvi (1983) estimates that 55×10^9 m^2 of the original 104×10^9 m^2 of wetlands have been reclaimed since PIH.

United Kingdom. As much as half of the lowland fens and mires of United Kingdom have been lost by exploitation (Williams, 1990); their present-day area is estimated to be 27×10^9 m^2 (Taylor, 1983), leading to a potential PIH cover of 54×10^9 m^2.

Australasia. The reclamation in the New South Wales, Western and South Australia and Victoria led to a loss of about 60% of the natural wetlands (Campbell, 1983). With 104×10^9 m^2 of wetlands in these four states today (from the data of Matthews and Fung, 1987), we obtain a PIH wetland area of 260×10^9 m^2 in the South of Australia.

South-Southeast Asia. For the 1880 period, Flint and Richards (1993) estimate a wetland surface of 422×10^9 m^2 in a studied area including Northern India, Bangladesh, Burma, Thailand, Malaysia, Brunei and Indonesia. By the 1980's, the figure decreases to 270×10^9 m^2.

Globally the exploitation amounted to 1020×10^9 m^2, so that the global wetland area for the PIH is 6260×10^9 m^2. As can be expected from the data sources, the wetland depletion occurred mainly in Northern mid-latitudes (30°N–60°N), totalling there 657×10^9 m^2.

To obtain the wetland distribution for the PIH, we assumed that the increase in wetland areas for each vegetation type in each country/region is proportional to today's distribution of the vegetation types within that country/region. The frequency distribution of wetland areas in different slope classes for each vegetation group is kept identical for today and PIH.

As a consequence of the wetland areal change between PIH and today, the distribution of PIH wetlands among vegetation groups differs from today's distribution: 56% of wetland depletion takes place in temperate broad-leaved forests and the other 44% occurs equally between tropical moist forests, tropical scrub/woodlands and boreal/conifer forests. Accordingly, the fraction wetland/vegetation increases from 3.3% (today) to 7.8% (PIH) in temperate broad-leaved forests, and reaches 4.2, 6.0 and 9.1% in tropical scrub/woodlands, tropical moist forests and boreal/conifer forests, respectively.

Note that uncertainties must surround the estimates of wetland area of the PIH. First, there is little historical information available for other parts of the world (especially China, Africa and South America). Second, evolving methods of investigation, wetland classification, and purpose of survey in the available inventory studies do not allow for precise interpretation of areal change.

2.1.3. Distribution of wetlands for LGM. By applying the PIH wetland/vegetation/slope relationship presented in Table 1 to the vegetation and slope distribution for the LGM, we obtained the distribution of wetlands for the LGM (Figs. 1a and 3). A category "southern steppe-tundra" was created by Adams et al. (1990) to account for a widespread vegetation type with no present analogue; its composition suggesting a similarity with dry tundra and polar desert, we assume that it was wetland-free. Because of the colder and generally drier climate during the LGM, there is a 55–60% reduction of tropical forests and woodlands. Temperate and boreal forests and woodlands, which have the largest areal expanse of wetlands for today's climate, occupied only 15% of today's area. According to Adams et al. (1990), the tundra vegetation had no analogue during the LGM.

These changes of vegetation coverage between PIH and LGM lead to a decrease by 58% of the global wetland area, totalling then 2615×10^9 m^2. The large wetland reductions concern these associated with tropical, temperate and boreal forests/woodlands as well as tundra. The use of the terrain slope as a constraint on wetland occurrence modulates the vegetation effect alone. For instance, tropical forests are reduced globally by 59% but they developed on the flat continental shelves of Southeast Asia; therefore, wetlands associated with this vegetation group were reduced by only 52%. When removing the slope constraint on wetland occurrence, the vegetation change

from PIH to LGM alone leads to a decrease of the global wetland coverage by 62%; thus vegetation alone drives much of the wetland areal change.

2.1.4. Changes in wetland latitudinal distribution. Fig. 1b presents the distribution of wetland areas as a function of latitudinal bands of 10°, for today, PIH and LGM. Northward from 40°N, the wetland extent during the LGM is considerably reduced as an effect of ice sheet growth on what is now large peat basins. Between 40°N and 20°N, there is a small expanse of wetlands linked to the existence of conifer forests and woodlands around the China Sea and south of the Laurentide ice sheet (Fig. 3). Southward, the wetland coverage is generally decreased. On the global decrease of 58% of the wetland area from PIH to LGM, 42% of the decrease take place south of 20°N and 58% occur in high/middle north latitudes.

2.1.5. Estimation of methane emission. Annual emission of methane from wetlands depends on the duration of inundation or methane production and the rate of methane escape to the atmosphere during this period. Fung et al. (1991) constructed a global model that estimated both emission seasons and emission rates based on the climatology of monthly surface air temperature and precipitation. For regions experiencing freeze/thaw cycles, the emission season begins when monthly mean surface temperature rises above 5°C and snow cover vanishes; the season ends when temperature falls below 0°C. For other regions, the emission season corresponds to the months when mean precipitation exceeds mean potential evaporation. For high-latitude bogs, methane fluxes were assumed to be governed primarily by temperature and were calculated using relationships derived from field measurements. For tropical wetlands, the methane flux was assumed to be constant during the emission period.

The model was applied to each 1° grid containing wetlands in the data base of Matthews and Fung (1987), and resulted in emissions of 30 Tg/yr from high-latitude bogs, 5 Tg/yr from dry tundra and 80 Tg/yr from middle and low latitude wetlands.

The wetland association with vegetation groups is then used to calculate a mean annual flux of methane associated with each vegetation type (Table 2). The resulting distribution reveals a trend toward decreasing annual fluxes from low to high latitudes: the highest values are associated with tropical forests whereas tundra regions experience the lowest annual CH_4 fluxes. Conifer forests and woodlands, which include the largest wetland areas, emit little methane on an annual basis. Therefore the CH_4 emission from tropical forests is even higher than from boreal forests (Table 2).

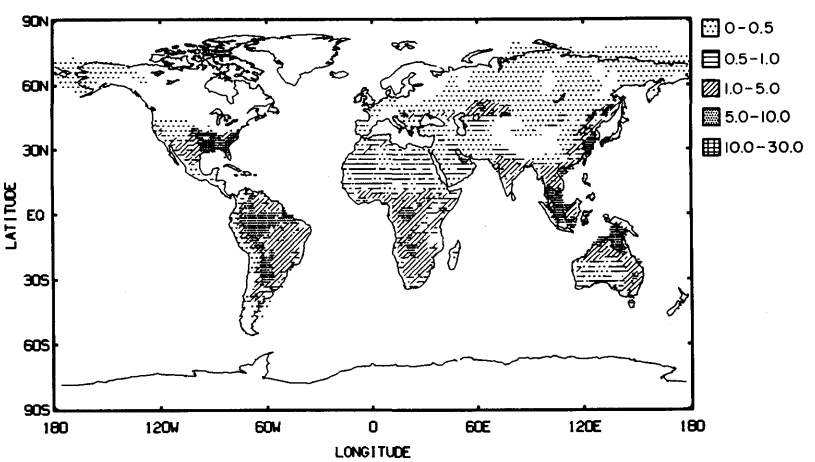

Fig. 3. Global map of wetland areal distribution during the Last Glacial Maximum, expressed as a fractional occurrence at 1° resolution. 6 classes are represented: ice (white); 0–0.5% (wide dots), 0.5–1.0% (wide horizontal lines), 1–5% (diagonal lines) and 5–10% (dense dots), >10% (up to 27%; cross-lines).

Table 2. *Annual CH_4 flux, area and CH_4 emission of wetlands in each vegetation group and for today, the Pre-Industrial Holocene (PIH) and the Last Glacial Maximum (LGM)*

Vegetation type (Adams et al., 1990)	CH_4 flux ($g\ m^{-2}\ yr^{-1}$) today (PIH)	Wetland area ($10^9\ m^2$) today	PIH	LGM	CH_4 emission (Tg/yr) today	PIH	LGM
tropical moist forest	46.1 (43.8)	589	741	357	27	33	16
tropical scrub/woodland	28.7 (27.4)	863	988	500	25	27	14
grassland	39.7 (39.7)	531	531	839	21	21	33
semi-desert/steppe	13.9 (13.9)	138	138	158	2	2	2
temperate broad-leaved forest	21.3 (19.5)	426	1001	270	9	20	5
boreal/conifer forest	11.6 (11.7)	1266	1434	110	15	17	1
open conifer woodland	7.9 (7.9)	732	732	215	6	6	2
tundra	6.0 (6.0)	596	596	0	8*	8	0
polar desert	0.0 (0.0)	0	0	0	0	0	0
ice	0.0 (0.0)	0	0	0	0	0	0
desert	19.8 (19.8)	99	99	167	2	2	3
southern steppe/tundra	0.0 (0.0)	0	0	0	0	0	0
global		5240	6260	2615	115	136	76

The annual flux is assumed identical for PIH and LGM.

* The present-day source of 5 Tg/yr from dry tundra is included in the CH_4 emission from the tundra vegetation group.

To obtain the PIH wetland source, we calculated the mean annual flux arising from today's wetlands in the country/regions with wetland exploitation, and we applied it to the extra PIH wetlands in each country/region. Globally this results in a wetland source strength of 135 Tg/yr (+17%). The emission from wetlands associated with temperate forests is more than doubled, reaching 20 Tg/yr (Table 2). The incorporation of extra PIH wetlands changes slightly the mean annual flux calculated for each vegetation group (Table 2). These PIH fluxes are the basis for the estimation of the LGM wetland source, as described below.

For the LGM, climatological information needed by the Fung et al., model is not available from paleodata. As already noted above, the modelled climate for the LGM is uncertain and does not fit well with the vegetation distribution reconstructed from paleodata (Prentice and Fung, 1990; Adams et al., 1990). Therefore we assume that the mean annual flux of methane attributed to each wetland/vegetation categories for PIH remained identical during the LGM. This is not unreasonable because a given vegetation can exist only under a limited range of climatic conditions and our approach implies unchanging climatic conditions for each wetland/vegetation category. For each vegetation type, the LGM wetland source is then the product of the PIH mean annual flux and the LGM wetland area.

The resulting LGM source strengths are shown in Table 2. Globally there is a 44% reduction of the wetland source, totalling 75 Tg/yr. The decrease in CH_4 emission is slightly smaller than the reduction in wetland area, due to the relatively high annual emission from grassland-associated wetlands, which expanded by 58%.

The latitudinal distribution of the wetland source is also largely changed: during PIH, 60% of the emissions occur in the Northern Hemisphere and the latitudinal profile presents two bands, between 70°N–30°N and between 10°N–40°S; on the other hand during LGM, the wetland emissions are about equally distributed between the Northern and Southern Hemispheres (47% and 53% respectively) and 63% arise from the Tropics between 10°N–20°S. The Northern mid and high latitudes experience a reduction of CH_4 emission of 43 Tg/yr whereas the decrease in regions south of 20°N is smaller, −17 Tg/yr.

2.2. *Other CH_4 sources*

Non-wetland natural sources include wild animals, termites, natural fires, oceans, freshwater and CH_4 hydrates (Table 3). During the latest part

Table 3. *Methane natural budgets for today, the Pre-Industrial Holocene, and the Last Glacial Maximum. Unit is Tg CH_4/yr*

Source/sink	Present*	Preindustrial Holocene	LGM
wetlands	115	135	75
wild animals	2–6	15	20
termites	20	20	20
wildfires	5	5	5
ocean/freshwater	10	10	10
CH_4 hydrates	5	5	0
soil sink	−10	−10	−10
total	150	180	120

* For present-day, human activities (domestic animals, rice cultivation, landfills, gas and coal exploitation, and human-induced fires) add another 340 Tg CH_4/yr (Fung et al., 1991).

of the PIH, some anthropogenic sources (rice cultivation, domestic animals) may have added to these natural sources. If we assume that they were proportional to the human population, they would amount to 20 Tg CH_4/yr. However during most of the PIH, the agricultural impact on the CH_4 budget was probably negligible and we will not consider these anthropogenic sources in our PIH budget.

Wild animals. The present-day CH_4 source from wild animals has been estimated to 2–6 Tg CH_4/yr (Crutzen et al., 1986), with the main contribution from tropical regions. Assigning a PIH figure is tentative as no global inventory exists; however, large-scale hunting and the shrinking of wildlife habitats probably led to a large decrease of wild animal populations since the last century. For instance, 50 to 70 million bisons were living in North America before European settlement and large populations existed in Eurasia. Considering a PIH global population equivalent to the current buffalo population (120 million; Crutzen et al., 1986) and the same CH_4 production per individual (same biological family), gives a PIH source from bison of 6 Tg CH_4/yr. Therefore, we estimate here a global PIH source of CH_4 from wild animals of 15 Tg/yr.

For LGM, we assume a linear relationship between animal populations and the extent of tropical/temperate grasslands, their main habitat. The reconstructed LGM landscape leads to an increased occurrence of grassland by ~50%, which implies a LGM source from wild animals of about 20 Tg CH_4/yr.

Termites. The PIH termite source is considered identical to present-day (20 Tg CH_4/yr, Fung et al., 1991), as cultivated areas in undeveloped countries and the ecosystems they replaced are both associated with termites. About 41% of this source emanates from savannas and 35% from tropical forests (Zimmerman et al., 1982; Fraser et al., 1986). During the LGM, the increase in savannas was accompanied by a decrease in tropical forests, resulting in no significant change in the areal extent of termite habitat. The LGM termite source remains at 20 Tg CH_4/yr.

Wildfires. At most, 10% of the biomass burning today is naturally induced (Crutzen and Andreae, 1990). This gives a PIH source of 5 Tg CH_4/yr using the value of Fung et al. (1991) for today. The parameters controlling the frequency and strength of wildfires are mainly the type of vegetation, the frequency of lightning (not associated with heavy rainfall) and the water stress on vegetation (drought). The last two ones being unconstrained, the CH_4 source for LGM is kept constant at 5 Tg/yr.

Other sources. Emissions from ocean, freshwater and CH_4 hydrates are perturbed primarily by climate, and not by human activities. We therefore kept their PIH emissions at today's levels. For the LGM, the increased solubility of CH_4 in the colder ocean, the higher concentration gradient between the atmosphere and the open water, and the decreased surface of the global ocean (increased sea-ice extent and lower sea-level) may compensate each other, and so this source is kept at 10 Tg CH_4/yr. However, the colder climate is likely to enhance the stability of hydrates, whose source strength we reduced to zero.

2.3. *Soil sink*

The present-day global soil uptake is considered here as only −10 Tg CH_4/yr (Fung et al., 1991). As absorption rates are low in cultivated soils (Keller et al., 1990; Mosier et al., 1991), the PIH soil sink should be higher than today, but the difference can be neglected with a sink strength of −10 Tg CH_4/yr. The soil sink is strongest in sandy soils, which underlie temperate and boreal forests,

and deserts (Born et al., 1990; Whalen et al., 1991; Delmas et al., 1992; Dörr et al., 1993). The large decrease in boreal forests and large increase of desert area in the reconstructed landscape thus results in little change in the LGM soil sink from the PIH value, that is -10 Tg CH_4/yr.

2.4. *Summary budget*

Globally, we propose a PIH CH_4 source (minus the soil sink) of 180 Tg/yr (Table 3), with a main contribution from wetlands (75%). For LGM, we obtain a smaller source of 120 Tg CH_4/yr, with a wetland contribution down to 63%.

3. Photochemical model calculations

A multibox one-dimensional model (Thompson et al., 1990) is used to calculate atmospheric CH_4 profiles compatible with the PIH and LGM sources. Besides CH_4, the model simulates 24 other trace gases and transients, including OH, O_3, CO, NO and H_2O_2 (hydrogen peroxide). The kinetics scheme used in the model is described in Thompson and Cicerone (1986); an updated rate coefficient for the reaction between CH_4 and OH is taken from Vaghjiani and Ravishankara (1991). The model boxes represent 6 chemically distinct environments (e.g., continental and marine northern mid-latitudes, tropical and southern hemisphere marine regions) spanning 63°N to 63°S and covering ~90% of the surface area of the globe. The model is initialized for 1990 conditions by adjusting model fluxes of CH_4, CO and NO to reproduce present-day surface mixing ratios of NO_x, CO, CH_4, O_3, and OH typical of each region. There is no interbox transport; therefore model fluxes represent the net fluxes resulting from surface and interbox exchange. The 440 Tg CH_4/yr flux thus deduced is somewhat lower than the sources used in the Fung et al. (1991) 3-D model budget. Concentrations and budgets reported refer to global means or fluxes obtained by averaging over the six regions and scaling up to total Earth area. Mean surface values of CO, NO_x, and O_3, and the global abundance of OH are given in Table 4.

To include the range of CH_4 levels from the LGM up to present-day, calculations are made with CH_4 fluxes introduced incrementally from 110 to 550 Tg/yr. Besides forcing by CH_4 sources, we must consider atmospheric O_3, H_2O, CO and NO whose reactions with OH affect the lifetime of CH_4 in the atmosphere. The sources of CO and NO have also increased since preindustrial times but in ways more difficult to quantify than CH_4. They are parameterized in the model calculations by simulating total CO budgets from 110–880 Tg C/yr and NO from 5.5–44 Tg N/yr. The higher ends of these ranges represent typical budgets for present-day conditions (Khalil and Rasmussen, 1990; Logan, 1983); the lower ends are reasonable for pristine atmospheres. The NO and CO budgets are scaled together because most of their sources (combustion, biomass burning, ocean and soils) are similar. Fig. 4 shows model-calculated CH_4 mixing ratios as a function of CH_4, CO and NO fluxes. The LGM CH_4 mixing ratio, 350 ppbv (Stauffer et al., 1988; Chappellaz et al., 1990) is consistent with a CH_4 flux of 110–130 Tg/yr, close to the LGM budget from paleodata and reconstructed vegetation (Table 4). When model runs are repeated with temperature profiles appropriate for LGM conditions (-4.5 K at the surface, Hansen et al., 1984), the CH_4 fluxes supporting 350 ppbv CH_4 are 100–110 Tg/yr.

Table 4. *Photochemical model input and output*

	Present*	Preindustrial Holocene	LGM
	model input		
CH_4 flux (Tg/yr)	440	190	110
CO flux (Tg C/yr)	770	440	110
NO flux (Tg N/yr)	39	22	5.5
temperature (K)	288.2	288.2	283.7
	model output (Global mean, 0 km)		
CH_4 (ppbv)	1800	700	350
CO (ppbv)	120	50	16
NO_x (pptv)	260	90	33
O_3 (ppbv)	27	16	11
OH (10^{11} molec · cm^{-2}) (0–15 km)	9.3	11.5	12.2

* Details of regional fluxes and mixing ratios are given in Thompson et al. (1993).

4. Discussion

In this study, an effort is made to quantify changes of the wetland CH_4 source and other

minor sources, from the Last Glacial Maximum to the present. Historical information is used to estimate the anthropogenic impact on the global flux of methane since the preindustrial Holocene; two correlates, vegetation and topography, of the wetland distribution provide an estimate of the wetland coverage and activity during the LGM, and the vegetation is also used to estimate other sources. These estimates result in a global flux of 180 Tg/yr for the PIH and 120 Tg/yr for the LGM, implying a residence time of CH_4 of 11 and 8 years respectively.

This approach is currently the only way of quantifying CH_4 sources prior to the large-scale anthropogenic impact on the CH_4 cycle. However, some caveats accompany our budgets: (1) they depend on the present-day strength and distribution of each component of the budget; these are somewhat uncertain and further revision of PIH and LGM budgets could result from improving knowledge of today's CH_4 cycle; (2) uncertainties surround the estimate of wetland exploitation since PIH, due to an incomplete coverage of the globe and to changing method and classification used in the available inventory studies; (3) we assume that the present-day relationship between wetland, vegetation and topography remained identical through time, although other parameters such as soil texture and permeability could modify this link; (4) PIH wild fires and animals are poorly constrained as no inventory exists; (5) the LGM vegetation map is reconstructed from sporadic paleodata whose quality has not been asserted unequivocally, and there is clearly some arbitrariness in drawing vegetation boundaries. However when tested in a one-dimensional multi-box photochemical model, the PIH and LGM fluxes reproduce the load of CH_4 in the interglacial and glacial atmosphere fairly well.

The change in CH_4 sources from PIH to LGM is dominated by variations in wetland contribution, which decreased by about a half from interglacial to glacial conditions. Note that the dominant role of wetlands was already hypothesized qualitatively in previous works (Stauffer et al., 1988; Raynaud et al., 1988; Khalil and Rasmussen, 1989; Chappellaz et al., 1990). In our quantitative analysis, the decrease dominated in the Northern mid and high latitudes, where the decrease is 43 Tg/yr compared to 17 Tg/yr for regions south of 20° N. In analysis of the longer time series of methane variations, however, it has been inferred that it was precipitation changes at low latitudes, more so than variations in ice sheet extent over North America and Europe, that caused the methane variations during the last glaciation (Chappellaz et al., 1990; Petit-Maire et al., 1991; Street-Perrott, 1992). This apparent differing inference about the region dominating the methane change may lie in the dynamics of the wetland distribution from the Holocene Climatic Optimum (9 kyr BP) to the PIH about 200 years ago. Both paleodata and models point to a stronger African–Asian monsoon from 12 to 6 kyr BP than during the present time, due to an increased seasonality of solar radiation during the Early Holocene (COHMAP Members, 1988). Therefore, tropical wetland extent may have been larger at the end of the deglaciation than during the PIH, and so a PIH–LGM comparison may indeed underestimate the role of the tropics during deglaciation. Clearly, evolutive and global vegetation maps from paleodata would be most helpful to ascertain the relative roles of low and high latitudes in CH_4 changes throughout the glacial-interglacial transitions.

On the atmospheric part of the CH_4 budget, calculations done with the photochemical model reveal a weaker effect of CO and NO_x sources on the CH_4 source/concentration relationship at smaller sources of CH_4. For the LGM, the difference between CH_4 mixing ratios calculated with the scenario that assumes only CH_4 source changes and scenarios assuming CH_4-CO-NO changes is only 30 ppbv CH_4 (Fig. 4), which is roughly the uncertainty of the ice core CH_4 measurements (Chappellaz et al., 1990). In other words, although OH (and lifetime) changes for CH_4 are important, CH_4 changes appear to be driven primarily by changes in CH_4 sources. The fact that CH_4 flux changes are able to explain a large part of CH_4 increases from the Last Glacial Maximum to the present is due to feedback effects involving atmospheric OH, the abundance of which is largely controlled by CH_4 levels.

The effect of CH_4 source reductions on OH, CO and O_3 is not negligible either. Table 4 shows that methane changes in the pre-industrial Holocene could have meant a 24% higher global OH abundance, consistent with 23% less CO and 41% less O_3. Unfortunately there are no records of CO and O_3 with which to compare these results.

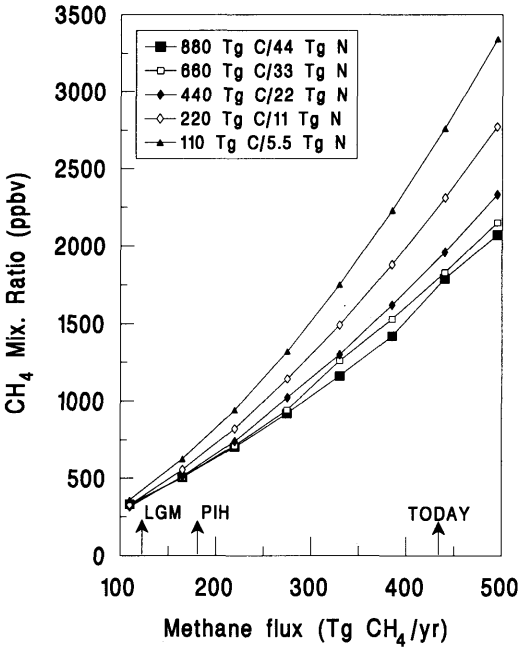

Fig. 4. Steady-state CH_4 concentration obtained by the one-dimensional photochemical model as a function of surface CH_4, CO and NO fluxes.

The dominance of the CH_4 source in setting CH_4 levels has been pointed out in other model analyses of LGM CH_4 levels (McElroy, 1989; Pinto and Khalil, 1991; Valentin, 1990), although these models use different fluxes to fit the ice-core record of CH_4. For example, with a one-dimensional model and LGM temperature, Pinto and Khalil (1991) deduce a flux of 90 Tg CH_4/yr; McElroy (1989) reports 180 Tg CH_4/yr for 350 ppbv inferred with a one-dimensional model at present-day temperature. A two-dimensional model, which differs from our model's present-day CH_4 flux by less than 10%, yields 180 Tg CH_4/yr for the LGM (Valentin, 1990). The large range among the models is also found for PIH conditions (see Thompson et al., 1993, for discussion). Some of these discrepancies probably result from model differences in CO, NO and OH distributions, as well as other physical features of the models. Using the ice core CH_4 record to evaluate which assumptions about historic emissions are realistic gives only one constraint against which to gauge the models. Unfortunately, for trace gases other than CH_4 that have been measured in ice cores (e.g., HCHO, H_2O_2, methanesulfonic acid) interpretation of the record is even more difficult.

5. Summary and conclusions

The pre-industrial source of CH_4 from wetlands has been estimated and added to budgets for other activities to give total CH_4 fluxes. Human impacts on the biosphere since the beginning of industrialization are evaluated to deduce a wetland coverage of 6260×10^9 m^2, a wetland emission of 135 Tg CH_4/yr and a total CH_4 source of 180 Tg/yr for the pre-industrial Holocene.

Correlations between wetlands and slope of terrain and between wetlands and vegetation types have been used with a global vegetation map for the LGM to deduce a wetland surface of 2615×10^9 m^2 and a wetland emission of 75 Tg CH_4/yr for this period. Combined with other natural source estimates, we deduce a LGM source of 120 Tg CH_4/yr.

Uncertainties on these estimates arise from assumptions on today's budget and the use of proxy data to deduce PIH and LGM CH_4 emissions. Improving knowledge of present-day fluxes and terrain characteristics during the LGM may help to reduce these uncertainties in the future.

Incorporation of our CH_4 sources for the PIH and LGM periods into a photochemical model gives CH_4 levels in good agreement with observations of ice cores CH_4. This is in large measure due to the feedback between OH and CH_4 regardless of assumptions made about historic CO and NO fluxes. However, these sources are near the lower end of published estimates deduced from other photochemical models.

Future measurements of reactive trace species (CH_3Cl, OCS) in ice cores may help to further constrain model results. Also a test of the CH_4 budgets inferred in this study would be to perform isotopic measurements of CH_4 in ice cores.

6. Acknowledgments

We thank T. Kucsera and J. John for computing assistance, C. Genthon for drafting help in figure 3, and E. Matthews, J. Pinto and K. Prentice for

discussion. The support of the NASA Biospherics Research Program, NASA Biogeochemistry and Geophysics Program, NASA EOS Interdisciplinary Science Branch and US Environmental Protection Agency are acknowledged. The Goddard Earth Sciences Directorate funded travel between New York and Greenbelt. This research was carried out while J.A.C. was a National Research Council Resident Research Associate at NASA Goddard Institute for Space Studies.

REFERENCES

Adams, J. M., Faure, H., Faure-Denard, L., McGlade, J. M. and Woodward, F. I. 1990. Increases in the terrestrial carbon storage from the Last Glacial Maximum to the present. *Nature 348*, 711–714.

Armentano, T. V. and Menges, E. S. 1986. Patterns of change in the carbon balance of organic soil-wetlands of the temperate zone. *J. Ecology 74*, 755–774.

Aselmann, I. and Crutzen, P. J. 1989. Global distribution of natural freshwater wetlands and rice paddies, their net primary productivity, seasonality, and possible methane emissions. *J. Atmos. Chem. 8*, 307–358.

Blake, D. R. and Rowland, F. S. 1988. Continuing worldwide increase in tropospheric methane, 1978 to 1987. *Science 239*, 1129–1131.

Born, M., Dörr, H. and Levin, I. 1990. Methane consumption in aerated soils of the temperate zone. *Tellus 42B*, 2–8.

Botch, M. S. and Masing, V. V. 1983. Mire ecosystems in USSR (ch. 4). In: *Ecosystems of the world, (4B), vol. 2* (ed. A. J. P. Gore). Elsevier, Amsterdam, 95–152.

Campbell, E. O. 1983. Mires of Australia (Chp. 5). In: *Ecosystems of the world, (4B), vol. 2* (ed. A. J. P. Gore). Elsevier, Amsterdam, 153–180.

Chappellaz, J., Barnola, J. M., Raynaud, D., Korotkevich, Y. S. and Lorius, C. 1990. Ice-core record of atmospheric methane over the past 160,000 years. *Nature 345*, 127–131.

CLIMAP Project Members. 1981. Seasonal reconstruction of the Earth's surface at the Last Glacial Maximum. *Geol. Soc. Am. Map and Charts Series MC-36.*

COHMAP Members. 1988. Climatic changes of the last 18,000 years: observations and model simulations. *Science 241*, 1043–1052.

Craig, H. and Chou, C. C. 1982. Methane: The record in polar ice cores. *Geophys. Res. Lett. 9*, 1221–1224.

Crutzen, P. J., Aselmann, I. and Seiler, W. 1986. Methane production by domestic animals, wild ruminants and other herbivorous fauna, and humans. *Tellus 38B*, 271–284.

Crutzen, P. J. and Andreae, M. O. 1990. Biomass burning in the Tropics: impact on atmospheric chemistry and biogeochemical cycles. *Science 250*, 1669–1678.

Crutzen, P. J. and Zimmermann, P. H. 1991. The changing photochemistry of the troposphere. *Tellus 43AB*, 153–166.

Delmas, R. A., Servant, J., Tathy, J.-P., Cros, B. and Labat, M. 1992. Sources and sinks of methane and carbon dioxide exchanges in mountain forest in equatorial Africa. *J. Geophys. Res. 97*, 6169–6179.

Dörr, H., Katruff, L. and Levin, I. 1993. Soil texture parameterization of the methane uptake in aerated soils. *Chemosphere*, in press.

Fairbanks, R. G. 1989. A 17,000-year glacio-eustatic sea level record: influence of glacial melting rates on the Younger Dryas event and deep-ocean circulation. *Nature 342*, 637–642.

Flint, E. P. and Richards, J. F. 1993. A century of land use change in South and Southeast Asia. In: *Effects of land use change on atmospheric CO_2 concentrations: Southeast Asia as a case study* (ed. V. H. Dale). Springer-Verlag, New York, in press.

Fraser, P. J., Rasmussen, R. A., Creffield, J. W., French, J. R. and Khalil, M. A. K. 1986. Termites and global methane, another assessment. *J. Atm. Chem. 4*, 295–310.

Fung, I., John, J., Lerner, J., Matthews, E., Prather, M., Steele, L. P. and Fraser, P. J. 1991. Three-dimensional model synthesis of the global methane cycle. *J. Geophys. Res. 96*, 13033–13065.

Hansen, J., Lacis, A., Rind, D., Russell, G., Stone, P., Fung, I., Ruedy, R. and Lerner, J. 1984. Climate Sensitivity: Analysis of feedback mechanisms. In: *Climate processes and climate sensitivity. Geophys. Monograph 29, Maurice Ewing vol. 5* (eds. J. Hansen and T. Takahashi), AGU, Washington DC, 130–163.

Henderson-Sellers, A. and Wilson, M. F. 1983. Surface albedo data for climatic modeling. *Rev. Geophys. Space Physics 21*, 1743–1778.

Keller, M., Mitre, M. E. and Stallard, R. F. 1990. Consumption of atmospheric methane in soils of Central Panama. *Global Biogeochem. Cycles 4*, 21–27.

Khalil, M. A. K. and Rasmussen, R. A. 1982. Secular trends of atmospheric methane (CH_4). *Chemosphere 11*, 877–883.

Khalil, M. A. K. and Rasmussen, R. A. 1989. Climate-induced feedbacks for the global cycles of methane and nitrous oxide. *Tellus 41B*, 554–559.

Khalil, M. A. K. and Rasmussen, R. A. 1990. Atmospheric carbon monoxide: Latitudinal distribution of sources. *Geophys. Res. Lett. 17*, 1913–1916.

Logan, J. A. 1983. Nitrogen oxides in the troposphere: Global and regional budgets. *J. Geophys. Res. 88*, 10785–10807.

Matthews, E. 1983. Global vegetation and land use: New high-resolution data bases for climate studies. *J. Climate and Appl. Meteorol. 22*, 474–487.

Matthews, E. and Fung, I. 1987. Methane emission from natural wetlands: Global distribution, area and

environmental characteristics of sources. *Global Biogeochem. Cycles 1*, 61–86.

McElroy, M. B. 1989. Studies of polar ice: insights for atmospheric chemistry. In: *The Environmental Record in Glaciers and Ice Sheets* (eds. H. Oeschger and C. C. Langway). John Wiley and Sons, New York, 363–377.

Mitsch, W. J. and Gosselink, J. G. 1986. *Wetlands.* Van Nostrand Reinhold Comp., New York, 539 pp.

Mosier, A., Schimel, D., Valentine, D., Bronson, K. and Parton, W. 1991. Methane and nitrous oxide fluxes in native, fertilized, and cultivated grasslands. *Nature 350*, 330–332.

National Geophysical Data Center (NGDC). 1988. ETOP05, NOAA, Boulder, CO, USA.

Office of Technology and Assessment. 1984. Wetlands: their use and regulation. US Congress OTA-O-206, Washington DC, 208 pp.

Pearman, G. I., Etheridge, D., De Silva, F. and Fraser, P. J. 1986. Evidence of changing concentrations of atmospheric CO_2, N_2O and CH_4 from air bubbles in Antarctic ice. *Nature 320*, 248–250.

Petit-Maire, N., Fontugne, M. and Rouland, C. 1991. Atmospheric methane ratio and environmental changes in the Sahara and Sahel during the last 130 kyrs. *Palaeogeogr., Palaeoclim., Palaeoecol. 86*, 197–204.

Pinto, J. P. and Khalil, M. A. K. 1991. The stability of tropospheric OH during ice ages, interglacial epochs and modern times. *Tellus 43AB*, 136–151.

Prentice, K. C. 1990. Bioclimatic distribution of vegetation for general circulation model studies. *J. Geophys. Res. 95*, 11811–11830.

Prentice, K. C. and Fung, I. 1990. The sensitivity of terrestrial carbon storage to climate change. *Nature 346*, 48–51.

Rasmussen, R. A. and Khalil, M. A. K. 1984. Atmospheric methane in the recent and ancient atmospheres: concentrations, trends and interhemispheric gradient. *J. Geophys. Res. 89*, 11599–11605.

Rasmussen, R. A. and Khalil, M. A. K. 1986. Atmospheric trace gases: trends and distributions over the last decade. *Science 232*, 1623–1624.

Raynaud, D., Chappellaz, J., Barnola, J. M., Korotkevich, Y. S. and Lorius, C. 1988. Climatic and CH_4 cycle implications of glacial-interglacial CH_4 change in the Vostok ice core. *Nature 333*, 655–657.

Rind, D. and Peteet, D. 1985. Terrestrial conditions at the Last Glacial Maximum and CLIMAP sea-surface temperature estimates: are they consistent? *Quat. Res. 24*, 1–22.

Roe, H. B. and Ayres, Q. C. 1954. *Engineering for agricultural drainage.* McGraw-Hill, New York, 501 pp.

Ruuhijärvi, R. 1983. The Finnish mire types and their regional distribution (Chp. 2). In: *Ecosystems of the World, (4B), vol. 2* (ed. A. J. P. Gore). Elsevier, Amsterdam, pp. 47–67.

Shaw, S. P. and Fredine, C. G. 1956. Wetlands of the United States, their extent, and their value for waterfowl and other wildlife. US Department of Interior, Fish and Wildlife Service, Circular 39, Washington DC, 67 pp.

Spivakovsky, C. M., Wofsy, S. C. and Prather, M. J. 1990a. A numerical method for parameterization of atmospheric chemistry: Computation of tropospheric OH. *J. Geophys. Res. 95*, 18433–18439.

Spivakovsky, C. M., Yevich, R., Logan, J. A., Wofsy, S. C., McElroy, M. B. and Prather, M. J. 1990b. Tropospheric OH in a three dimensional chemical tracer model: An assessment based on observations of CH_3CCl_3. *J. Geophys. Res. 95*, 18441–18471.

Stauffer, B., Fischer, G., Neftel, A. and Oeschger, H. 1985. Increase of atmospheric methane recorded in Antarctic ice core. *Science 229*, 1386–1388.

Stauffer, B., Lochbronner, E., Oeschger, H. and Schwander, J. 1988. Methane concentration in the glacial atmosphere was only half that of the preindustrial Holocene. *Nature 332*, 812–814.

Steele, L. P., Fraser, P. J., Rasmussen, R. A., Khalil, M. A. K., Conway, T. J., Crawford, A. J., Gammon, R. H., Masarie, K. A. and Thoning, K. W. 1987. The global distribution of methane in the troposphere. *J. Atmos. Chem. 5*, 125–171.

Street-Perrott, F. A. 1992. Tropical wetland sources. *Nature 355*, 23–24.

Taylor, J. A. 1983. The peatlands of Great Britain and Ireland (Chp. 1). In: *Ecosystems of the world, (4B), vol. 2* (ed. A. J. P. Gore). Elsevier, Amsterdam, 1–46.

Thompson, A. M. and Cicerone, R. J. 1986. Possible perturbations to tropospheric CO, CH_4, and OH. *J. Geophys. Res. 91*, 10853–10864.

Thompson, A. M., Huntley, M. A. and Stewart, R. W. 1990. Perturbations to tropospheric oxidants, 1985–2035: 1. Calculations of ozone and OH in chemically coherent regions. *J. Geophys. Res. 95*, 9829–9844.

Thompson, A. M., Chappellaz, J. A., Fung, I. Y. and Kucsera, T. L. 1993. The atmospheric CH_4 increase since the Last Glacial Maximum. 2. Interactions with oxidants. *Tellus 45B*, 242–257.

Vaghjiani, G. L. and Ravishankara, A. R. 1991. New measurement of the rate coefficient for the reaction of OH with CH_4. *Nature 350*, 406–409.

Valentin, K. M. 1990. Numerical modeling of the climatological and anthropogenic influences on the chemical composition of the troposphere since the Last Glacial Maximum. Ph. D. Thesis, Johannes-Gutenburg-Univ. Mainz, FRG, 1990.

Whalen, S. C., Reeburgh, W. S. and Kizer, K. S. 1991. Methane consumption and emission by taiga. *Global Biogeochem. Cycles 5*, 261–273.

Williams, M. 1990. *Wetlands: a threatened landscape.* Blackwell, Oxford, UK, 419 pp.

Zimmerman, P. R., Greenberg, J. P., Wandiga, S. O. and Crutzen, P. J. 1982. Termite: a potentially large source of atmospheric methane, carbon dioxide and molecular hydrogen. *Science 218*, 563–565.